

# 1 A Queueing-Theoretic Framework for Dynamic Attack 2 Surfaces: Data-Integrated Risk Analysis and Adaptive Defense 3

## 4 ANONYMOUS AUTHORS 5

6 We develop a queueing-theoretic framework to model the temporal evolution of cyber-attack surfaces, where  
7 the number of active vulnerabilities is represented as the backlog of a queue. Vulnerabilities arrive as they are  
8 discovered or created, and leave the system when they are patched or successfully exploited. Building on this  
9 model, we study how automation affects attack and defense dynamics by introducing an AI amplification  
10 factor that scales arrival, exploit, and patching rates. Our analysis shows that even symmetric automation  
11 can increase the rate of successful exploits. We validate the model using vulnerability data collected from  
12 an open source software supply chain, and show that it closely matches real-world attack-surface dynamics.  
13 Empirical results reveal heavy-tailed patching times, which we prove that they induce long-range dependence  
14 in vulnerability backlog and help explain persistent cyber risk. Utilizing our queueing abstraction for the  
15 attack surface, next we build a systematic approach for cyber risk mitigation. Toward that end, we formulate  
16 the dynamic defense problem as a constrained Markov decision process with resource-budget switching-  
17 cost constraints, and develop a reinforcement-learning (RL) algorithm that achieves provably near-optimal  
18 regret. Numerical experiments validate the approach and demonstrate that our adaptive RL-based defense  
19 policies significantly reduce successful exploits and mitigate heavy-tail queue events. Using trace-driven  
20 experiments on the ARVO dataset, we show that the proposed RL-based defense policy reduces the average  
21 number of active vulnerabilities in a software supply chain by over 90% compared to existing defense practices,  
22 without increasing the overall maintenance budget. Our results allows defenders to fundamentally quantify  
the cumulative exposure risk under long-range dependent attack dynamics and to design adaptive defense  
strategies with provable efficiency.

23 CCS Concepts: • Security and privacy → Vulnerability management; • Computing methodologies →  
24 Markov decision processes; Model verification and validation; Reinforcement learning.  
25

26 Additional Key Words and Phrases: computer security, vulnerability dynamics, queueing theory, reinforcement  
27 learning, long-range dependence

28 **ACM Reference Format:**

29 Anonymous Authors . 2026. A Queueing-Theoretic Framework for Dynamic Attack Surfaces: Data-Integrated  
30 Risk Analysis and Adaptive Defense. In *Proceedings of Make sure to enter the correct conference title from your*  
31 *rights confirmation email (Conference acronym 'XX)*. ACM, New York, NY, USA, 24 pages. <https://doi.org/XXXXXX.XXXXXXX>

32 **1 Introduction**

33 Cyber risk exhibits temporal dependence and cannot be adequately described by static or stationary  
34 reliability models. Much of the existing approaches in cybersecurity focus on isolated attack models  
35 or mitigation mechanisms, offering limited understanding of the holistic and time-varying nature  
36 of vulnerabilities that define an organization's *attack surface*. Modern infrastructures, spanning

---

37 Author's Contact Information: Anonymous Authors.

38 Permission to make digital or hard copies of all or part of this work for personal or classroom use is granted without fee  
39 provided that copies are not made or distributed for profit or commercial advantage and that copies bear this notice and the  
40 full citation on the first page. Copyrights for components of this work owned by others than the author(s) must be honored.  
41 Abstracting with credit is permitted. To copy otherwise, or republish, to post on servers or to redistribute to lists, requires  
42 prior specific permission and/or a fee. Request permissions from [permissions@acm.org](mailto:permissions@acm.org).

43 *Conference acronym 'XX, Woodstock, NY*

44 © 2026 Copyright held by the owner/author(s). Publication rights licensed to ACM.

45 ACM ISBN 978-1-4503-XXXX-X/2018/06

46 <https://doi.org/XXXXXX.XXXXXXX>

50 cloud services, software-defined networks, and distributed APIs, further amplify these dynamics,  
 51 producing attack surfaces whose scale and evolution are often unknown even to their operators.

52 To address this gap, we develop a *dynamic stochastic model* for the evolution of the attack  
 53 surface. The model generalizes from an individual software component to an entire organization,  
 54 and ultimately to large-scale ecosystems such as industry sectors or nation-state infrastructures.  
 55 We formalize the instantaneous size of the attack surface as the number of active vulnerabilities,  
 56 represented by the queue length of a stochastic service process. Arrivals to the queue correspond  
 57 to the discovery or creation of new vulnerabilities, while departures represent either (a) successful  
 58 exploitation or (b) successful patching. This queueing abstraction makes explicit the role of limited  
 59 defense capacity, allowing attack-surface management to be studied as a resource-allocation and  
 60 backlog-control problem.

61 Building on this foundation, we extend the model to capture the growing influence of automation  
 62 and AI in both offensive and defensive operations. We introduce an *AI amplification factor* that  
 63 scales vulnerability arrival, exploit, and patching rates. This abstraction is not intended to model AI  
 64 systems in detail, but to examine how this factor reshapes backlog dynamics. Our analysis shows  
 65 that even when attack and defense capabilities scale symmetrically, the rate of successful exploits  
 66 can still increase superlinearly.

67 To demonstrate how accurately our proposed framework captures real-world vulnerability  
 68 dynamics, we apply it to the problem of strengthening open-source software supply chains. Using the  
 69 ARVO (Atlas of Reproducible Vulnerabilities for Open Source Software) dataset [19], which contains  
 70 over 4,000 reproducible vulnerabilities from Google’s OSS-Fuzz platform, we characterize the real-  
 71 world dynamics of vulnerability discovery and patching across thousands of open-source projects.  
 72 Event-level analysis reveals that vulnerability arrivals and lifetimes are bursty, heavy-tailed, and  
 73 non-stationary, and that segmented queueing models accurately reproduce the temporal evolution  
 74 of the attack surface size across development cycles. This temporal structure further exhibits  
 75 *long-range dependence (LRD)*, indicating that correlations in exposure decay polynomially rather  
 76 than exponentially. In practical terms, the effects of individual vulnerabilities persist far beyond  
 77 their initial disclosure, highlighting systemic bottlenecks in patch deployment and motivating  
 78 the need for continuous, adaptive, and resource-aware defense strategies to ensure supply-chain  
 79 resilience.

80 Motivated by persistent patching delays and the imbalance between vulnerability arrivals and  
 81 limited defense capacity observed in both data and AI-driven analysis, we develop a reinforcement  
 82 learning (RL) approach for adaptive defense under resource-budget constraints. The defense re-  
 83 source, represented by the patching rate, directly influences the service process in our queueing  
 84 model. Our dynamic framework allows defense rates to vary over time, while explicitly incorpo-  
 85 rating such switching costs into performance evaluation. Although the resulting control problem  
 86 is analytically intractable in closed form, we design a low-complexity RL algorithm for adaptive  
 87 defense allocation under uncertainty. In addition, we rigorously establish a near-optimal regret  
 88 bound relative to an oracle defender and introduce new switching-reduction techniques that extend  
 89 the theory of constrained Markov decision processes (CMDPs).

90 Finally, to illustrate the practical implications of our theoretical and empirical findings, we  
 91 conduct numerical experiments to evaluate the proposed RL-based defense policy. The results  
 92 show that adaptive resource allocation guided by our RL algorithm can substantially mitigate  
 93 exploit success rates, achieving reductions of up to 55% compared to static defense strategies,  
 94 while maintaining stable performance under both stochastic and adversarial vulnerability arrivals.  
 95 In trace-driven experiments using the ARVO dataset, our adaptive defense policy reduces the  
 96 average number of active vulnerabilities in a software supply chain by more than 90% compared  
 97 to existing defense practices, while operating under the same overall maintenance budget. These

99 findings underscore that dynamic, learning-based defense policies not only outperform static  
 100 benchmarks, but also yield smoother and more predictable system behavior. This demonstrates  
 101 how our analytical framework can directly support real-world cyber-defense decision making.  
 102

103 *Contributions.* This work establishes a foundational framework for analyzing and controlling the  
 104 dynamics of organizational attack surfaces through a stochastic and queueing-theoretic lens. The  
 105 key contributions are as follows:

- 106 • **Dynamic Queueing Model of the Attack Surface.** We develop a queueing-theoretic  
 107 model that jointly captures the temporal and spatial evolution of active vulnerabilities,  
 108 providing a unified representation of vulnerability discovery, exploitation, and patching  
 109 across organizational or ecosystem scales.
- 110 • **AI-Amplified Threat Dynamics.** We extend the model with an *AI-amplification factor* that  
 111 quantifies how automation accelerates vulnerability creation and exploitation. Analytical  
 112 results show that the breach rate can grow superlinearly with automation, even when AI is  
 113 deployed defensively.
- 114 • **Empirical Validation and LRD of Vulnerability Dynamics.** Using the ARVO dataset,  
 115 we empirically validate the proposed queueing-theoretic framework on a real-world open-  
 116 source repository. By fitting segmented queueing models to vulnerability discovery and  
 117 patching events, we show that the model accurately captures the non-stationary and heavy-  
 118 tailed evolution of the attack surface. We further prove that such heavy-tailed service  
 119 distributions lead to LRD in attack surface size, explaining the persistent exposure patterns  
 120 observed in practice and highlighting the structural limits of static defense strategies.
- 121 • **Near-Optimal Adaptive Defense via RL.** We formulate adaptive patching as a CMDP with  
 122 resource-budget and switching-cost constraints, and develop a near-optimal RL algorithm  
 123 for adaptive defense. The algorithm achieves a sublinear regret relative to an oracle defender  
 124 and produces smoother, more stable defense actions under varying attack intensities.
- 125 • **Theoretical Advances in Learning-Based Defense.** Our analysis introduces switching-  
 126 reduction techniques and, to our knowledge, provides the first sublinear regret guarantees  
 127 for RL under the joint coexistence of resource-budget and switching-cost constraints. These  
 128 results advance the theoretical foundation of learning-based cyber defense.
- 129 • **Defense Switching Cost.** To our knowledge, this work is the first to model and analyze the  
 130 amount of defense change as a measurable switching cost in RL. Specifically, the switching  
 131 cost in Eq. (6) quantifies the *magnitude* of consecutive policy adjustments, in contrast to  
 132 previous approaches [2, 10, 26] that penalize only the *frequency* of policy changes.

133 Together, these contributions establish a quantitative and theoretically grounded foundation for  
 134 modeling, analyzing, and dynamically defending evolving attack surfaces.

## 135 2 Related Work

136 Our work is related to probabilistic approaches to cyber risk analysis. The industry standard,  
 137 Factor Analysis of Information Risk (FAIR) framework [12] formalizes cyber risk quantification  
 138 through probabilistic factors such as threat events, vulnerabilities, and loss magnitude, providing a  
 139 common language for risk assessment. Broader treatments of probabilistic cyber insurance and  
 140 risk evaluation can be found in [16]. While these approaches are influential, they largely assume  
 141 static system conditions and do not capture the evolving temporal dependencies characteristic of  
 142 modern attack surfaces.

143 The concept of the attack surface was formalized by Manadhata and Wing [18], and a systematic  
 144 review [29] revealed fragmented definitions across hundreds of studies. Recent large-scale analyses,  
 145 such as [9], quantified attack surfaces across government infrastructures, highlighting their scale  
 146

148 and complexity. These works provide valuable measurement perspectives, but they typically treat  
 149 the attack surface as a static quantity and do not model how it evolves over time or responds to  
 150 defense actions.

151 A related line of work models interdependent vulnerabilities through probabilistic attack graphs [30]  
 152 and their AI-based extensions [11]. Bayesian-network models [13, 23, 24] have been proposed to  
 153 estimate compromise probabilities, but these frameworks describe the system at a single snapshot  
 154 in time. We refer to such methods as *snapshot models of risk*, as they capture system state at a fixed  
 155 point in time and do not represent the sequential or long-range evolution of vulnerabilities.

156 Efforts to incorporate temporal evolution have used Bayesian networks for industrial and cloud  
 157 systems [25, 32] and Markovian models for sequential attacks [14, 17]. These studies focus on  
 158 specific environments rather than the evolution of the attack surface as a whole. Haldar and  
 159 Mishra [8] and Feutrill et al. [5] observed that vulnerability disclosures exhibit burstiness and  
 160 long-range dependence, suggesting queueing systems as a natural abstraction. However, existing  
 161 studies do not combine such models with large-scale empirical validation or address the joint  
 162 temporal and spatial dynamics of vulnerability backlogs.

163 A key enabler for such modeling is the availability of event-level vulnerability data. The recently  
 164 released ARVO dataset [19] provides detailed timestamps of vulnerability discovery and patching.  
 165 Our work is the first to leverage ARVO to calibrate and validate a queueing-theoretic model of  
 166 attack surface evolution, bridging theoretical abstractions with empirical vulnerability dynamics.

167 The rapid integration of AI into both software development and exploitation further complicates  
 168 this landscape. While large language models (LLMs) can assist in code repair [3, 28], they also  
 169 accelerate exploit generation [4, 7, 31]. Reports by practitioners and agencies [20, 22] highlight this  
 170 dual role of AI as both attacker and defender. Yet existing models do not provide a quantitative  
 171 framework for studying how automation simultaneously affects vulnerability discovery, exploita-  
 172 tion, and patching dynamics. Our use of an *AI amplification factor* is intended to capture these  
 173 rate-level effects in a tractable way.

174 Finally, constrained and safe RL has been studied under budget [1, 21, 27] and policy-adaptation  
 175 [2, 10, 26] constraints. Existing studies on policy-adaptation primarily penalize the number of  
 176 policy changes, i.e., the frequency of updates. Without the magnitude of change, it is not completely  
 177 possible to quantify the operational cost of change actions in practical defense settings. In contrast,  
 178 our formulation models the amount of change in the executed defense action and quantifies the  
 179 magnitude of consecutive policy adjustments. This distinction allows us to model reconfiguration  
 180 overhead in a more realistic way. Moreover, previous work does not consider the joint effect of  
 181 resource-budget and switching-cost constraints on adaptive defense policies. Our formulation  
 182 unifies these elements and provides the first theoretical regret guarantees for RL in this setting.

183 Overall, our study introduces a queueing-theoretic perspective that explicitly models the time-  
 184 varying and heavy-tailed nature of vulnerability backlogs. By validating the model on real data  
 185 and integrating it with adaptive control, we provide a quantitative framework for analyzing  
 186 dynamic attack surfaces and defense resource allocation. Using the framework, we provide an RL-  
 187 based systematic approach to allocating constrained defensive resources to achieve a significantly  
 188 improved attack surface dynamics, with the variations in the budget directly taken into account.

### 189 3 System Model

190 Consider a single component in an organization's IT stack, such as an authentication service, file  
 191 server, or endpoint device. Each component maintains an attack surface, which represents the **set**  
 192 of currently active vulnerabilities. For example, in a software release, the attack surface can  
 193 be defined as the set of unpatched bugs (the definition can also be extended depending on the  
 194 dependencies to the other systems). In a larger ecosystem, like an enterprise, the IT/OT environment

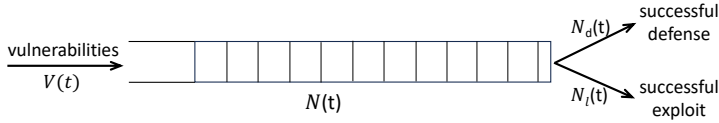


Fig. 1. Attack surface modeled as a queueing system. Vulnerabilities arrive via  $V(t)$  and depart through competing defense (patching) and exploit processes.

will have a complex attack surface, composed of the combination of the attack surfaces of each component in the system. The overall attack surface will exhibit an interplay across the network of components, and its size naturally reflects how many vulnerabilities remain exposed at a given time. In this paper, to build the initial foundation, we focus on a single subsystem or component. The single-component model can be naturally extended to multi-component or multi-organizational settings; we briefly discuss such extensions in Section 9.

The size of the associated attack surface at time  $t$  is represented by the stochastic process  $N(t)$ , which we model as the number of jobs in a queue. Here, arrivals correspond to the appearance of new vulnerabilities, and services represent their removal through patching or exploitation<sup>1</sup>. Let  $V(t)$  denote the arrival process of vulnerabilities, and  $N_d(t)$  and  $N_l(t)$  denote the cumulative numbers of defended and exploited vulnerabilities up to time  $t$ , respectively, as shown in Fig. 1. The discrete-time evolution of the attack surface size is given by

$$N(t+1) = \{N(t) + V(t) - [N_d(t) + N_l(t)]\}^+, \quad (1)$$

where  $\{\cdot\}^+ = \max\{\cdot, 0\}$ . Modeling the attack surface as a queue makes explicit the role of backlog: vulnerabilities accumulate when arrival rates exceed patching capacity, and shrink only when defenses can keep up. This recursion embodies the key intuition: new vulnerabilities enlarge the attack surface, while patching and exploitation act as concurrent removal mechanisms. As shown later in our empirical analysis (Section 6), both the arrival and lifetime processes exhibit burstiness, heavy-tailed persistence, and non-stationarity.

Each vulnerability is subjected to a *race condition* between defensive and offensive actions. Let  $D_d$  and  $D_l$  denote random variables representing the defense time and exploit time, respectively. For each active vulnerability,

$$D_s = \min\{D_d, D_l\}, \quad (2)$$

determines its completion time, and the winner of the race  $s = \arg \min\{D_d, D_l\}$  increments the corresponding counter  $N_s(t)$ . For instance, if  $D_d = 10^{-2}$  and  $D_l = 10^{-3}$  for a given vulnerability, the attacker acts ten times faster, leading to an exploit departure. This race captures the operational reality that a vulnerability remains exposed until either it is patched or it is exploited.

We define  $\mu_d(t)$  and  $\mu_l(t)$  as the instantaneous total mean service rates for the defense and exploitation processes, respectively. These rates quantify how quickly vulnerabilities are removed, either by defenders or attackers, at time  $t$ . Both sides may act on multiple vulnerabilities concurrently with the defensive limitation of simultaneous processing across  $m$  parallel servers under a fixed total capacity  $b$ . In practice, defensive prioritization or limited concurrency can be modeled by reducing  $m$  or adjusting per-server service rates. Here,  $b$  denotes the organization's defense budget, interpreted as the maximum aggregate patching effort that can be sustained at any time. Hence,

$$\mu_d(t) \leq b. \quad (3)$$

<sup>1</sup>Removal of a job upon exploitation is optional in the model. One may assume that a vulnerability can be exploited multiple times, before it is removed/patched from the surface queue.

These characteristics motivate the adoption of a general  $G/G/m-b$  model rather than simpler memoryless abstractions. Note that in Kendall's notation, the standard  $G/G/m/k$  framework [6] uses  $k$  to denote the maximum number of jobs allowed in the system (i.e., a queue-length capacity constraint). In contrast, our  $G/G/m-b$  notation utilizes  $m$  to denote the number of parallel servers and  $b$  to represent the aggregate capacity constraint imposed on the total service rate, effectively modeling resource-limited defense operations. This general model is necessary to capture bursty arrivals, heavy-tailed patching times, and hard capacity limits, which are not represented by memoryless queueing models.

Unlike classical queueing models with independent service rates, both  $\mu_d(t)$  and  $\mu_l(t)$  may depend on the current attack surface size  $N(t)$ . As  $N(t)$  grows, defenders must divide limited resources across more vulnerabilities, while attackers benefit from the expanded surface. This coupling creates a feedback effect: when the number of active vulnerabilities increases, the same defense capacity must be shared across more items, slowing down patching on each vulnerability, while attackers face more exposed targets and thus have more opportunities to succeed. For instance,  $\mu_d(t)$  may decrease inversely with  $N(t)$ , while  $\mu_l(t)$  increases proportionally to  $N(t)$ , reflecting the asymmetric scalability of attack versus defense. The interplay between these processes governs the temporal evolution of the attack surface.

**Variations of the Model:** Throughout this paper, we consider several specializations derived from our model:

- **Temporal variation analysis:** We use the limiting case  $M/G/\infty$ , which isolates temporal effects such as heavy-tailed persistence and LRD without capacity constraints, to build a theorem on how the heavy-tailed nature of the arrival and service processes affect the attack surface variations.
- **Data integration:** In Section 6, the model is instantiated as  $G/G/m-b$  in its full generality to capture bounded defense capacity and bursty vulnerability arrivals observed in the ARVO dataset.
- **Dynamic defense design and optimization:** In Section 8, we use the  $G/G/1-b$  variation to build the RL framework, where a single effective defense rate  $\mu_d(t)$  is adaptively controlled under resource and switching constraints.

## 4 Problem Formulation

Building on the stochastic queueing model above, we now formulate the adaptive defense problem. The objective is to allocate limited defense resources over time to minimize long-term exposure and breach costs, while accounting for reconfiguration (switching) overhead.

At each time step  $t$ , the defender selects a defense (patching) rate  $\mu_d(t)$  subject to the resource-budget constraint  $\mu_d(t) \leq b$ , while the effective exploitation rate  $\mu_l(t)$  evolves according to the coupled arrival-service dynamics defined earlier. The resulting queue length  $N(t)$  captures the number of active vulnerabilities and thus represents the instantaneous *attack surface size*. The control task is to design a policy  $\pi = \{\mu_d(t)\}_{t=1}^T$  that balances: (i) risk reduction through faster patching, (ii) efficiency in total resource use, and (iii) stability against frequent reallocations.

We study two core problems that together form the foundation of our framework. The first focuses on data-driven model inference and empirical validation, while the second develops an adaptive control policy for dynamic defense allocation. Each problem highlights a distinct analytical or algorithmic component of the overall approach:

### (P1) Data-Driven Characterization and Model Validation.

Given a set of event-level vulnerability data containing discovery and patch timestamps, we aim to find the optimal parameters  $\theta^*$  that minimize the statistical distance between

295 the empirical queue-length distribution (QLD), denoted by  $\hat{P}$ , and the simulated QLD,  $P(\theta)$ ,  
 296 generated by the candidate model. Formally, we define:  
 297

$$298 \min_{\theta \in \Theta} d(\hat{P}, P(\theta)) \quad (4)$$

300 where  $d(\cdot, \cdot)$  is a divergence metric, specifically the Kullback-Leibler (KL) divergence in  
 301 our implementation.  $\Theta$  is the parameter space for the  $G/G/m - b$  queueing model, where  
 302  $\theta = \{m, b, F_{IA}, F_{ST}\}$  includes the number of servers  $m$ , total capacity  $b$ , and the parametric  
 303 distributions for inter-arrival (IA) and service times (ST).

304 Solving (P1) yields a segmented and validated model that captures the non-stationary  
 305 and heavy-tailed behavior of real-world vulnerability dynamics, providing the empirical  
 306 foundation for the adaptive defense control in (P2).

307 **(P2) Learning-Based Adaptive Defense.** This problem aims to develop a learning policy that  
 308 adaptively controls  $\mu_d(t)$  to minimize cumulative cost, i.e.,

$$309 \min_{\{\vec{\mu}_d(1:T)\}} \sum_{t=1}^T \mathbb{E} \left[ C(\vec{N}_l(t)) + \|\vec{\mu}_d(t)\|_1 \right. \\ 310 \left. + g(\|\vec{\mu}_d(t) - \vec{\mu}_d(t-1)\|_\infty) \right] \quad (5)$$

311 sub.to:  $\vec{\mu}_d(t) \leq b, \quad t = 1, \dots, T,$

312 where  $\|\cdot\|_m$  represents the  $\ell_m$  norm. The expectation reflects stochastic variability in attack  
 313 arrivals and patching delays. The first term  $C(\vec{N}_l(t))$  penalizes exploit success proportional  
 314 to the instantaneous attack surface size, the second term  $\|\vec{\mu}_d(t)\|_1$  captures cumulative  
 315 resource use, and the third term  $g(\cdot)$  models the switching cost for defense reconfiguration.  
 316 Note that in contrast to abstract policy-adaptation cost in existing work, this switching cost  
 317 is proportional to the *magnitude* of change in executed actions. The  $\ell_1$  norm in the second  
 318 term captures the total defense effort expended over time, corresponding to cumulative  
 319 patching resources. In contrast, the  $\ell_\infty$  norm in the third term measures the largest change in  
 320 defense rate between consecutive time steps, reflecting the operational cost of reconfiguring  
 321 defense actions rather than the frequency of policy updates.

322 Before introducing adaptive defense strategies, we first analyze a few simple scenarios under  
 323 basic static allocation case to build some intuition on attack surface dynamics.

## 324 5 Illustrative Examples: Static Resource Allocation

325 We begin with a simple baseline that assumes a fixed defense allocation. This example is **not**  
 326 intended to represent a realistic situation, but rather to build intuition about how defense capacity  
 327 and vulnerability arrivals interact in a queueing system. In this example, we assume memoryless  
 328 arrivals and departures from our queue. These insights will help us better interpret the results in  
 329 the later sections, where we relax the memoryless assumption.

### 330 5.1 M/M/ $\infty$ Abstraction

331 The memoryless nature of the arrival and service processes with the M/M/ $\infty$  queue removes  
 332 temporal correlations and capacity interactions, allowing us to focus on how vulnerability arrivals  
 333 and fixed defense capacity jointly determine attack surface size and exploitation rates. The state of  
 334 the associated M/M/ $\infty$  system can be represented as a Markov chain with countable state-space.

335 As described in Section 3, in our analyses we assume that organizations have fixed amount of  
 336 cyber resources and allocate the full amount without a variation from one episode to another. In  
 337 particular, the rate of the successful defense process  $\mu_d = \alpha\lambda$  remains constant and thus independent

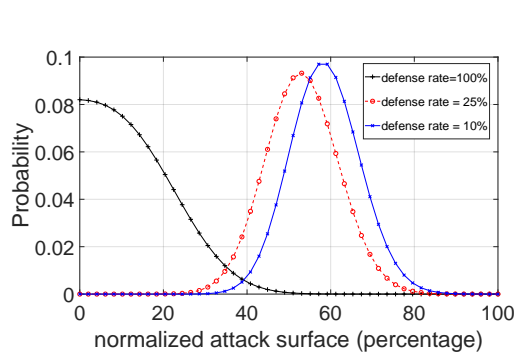


Fig. 2. Probability mass function for the size of the attack surface for different defense rates. Surface size is scaled 0–100% for visual interpretation.

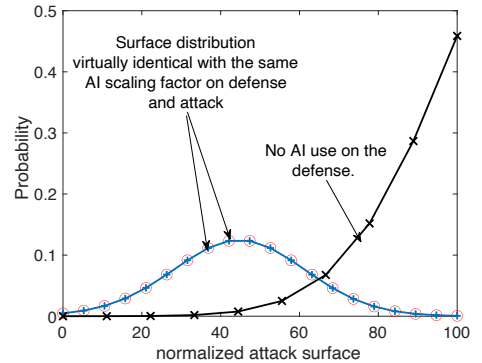


Fig. 3. Probability mass function for the size of the attack surface with AI usage. Distribution remains identical under symmetric AI scaling while a major degradation is observed with no AI use on the offense.

of  $N(t)$  where  $\lambda$  is the arrival rate for  $V(t)$ , the (stationary) vulnerability process, and  $\alpha$  is a constant such that  $\alpha\lambda \leq b$ . Here,  $\mu_d$  denotes the total defense rate. The variable  $\alpha$  signifies the intensity of the defense. As an example, if  $\alpha = 1$ , we say the defense rate is 100% or if  $\alpha = 0.5$ , we say the defense rate is 50%.

On the attacker side, we assume the rate of the successful exploitation process grows proportional to  $N(t)$  as a larger number of active vulnerabilities attracts more attack attempts targeting the exposed surface, growing proportional to the attack surface size. Hence,  $\mu_l(t) = \beta\lambda N(t)$ , where  $\beta$  is a constant denoting the intensity of attacks on the organization.

In Fig. 2, we illustrate the probability mass function (PMF) of the state of the attack surface. Here, we picked a constant and normalized the observed queue sizes with respect to that constant. As a result, the queue size is denoted as a “percentage” in the figure, rather than an absolute value. We took the vulnerability arrival rate as  $\lambda = 100$  per unit time and  $\beta = 0.001$ . We have plotted three different PMFs for different values of defense rate:  $\alpha = 100\%$ ,  $25\%$ , and  $10\%$ .

The curve with the full (100%) defense rate leads to a small expected surface size of  $\mathbb{E}[N(t)] = 13.2\%$  and a time-averaged breach rate of  $\lim_{t \rightarrow \infty} \frac{1}{t} \mathbb{E}[N_l(t)] = 6.79$  breaches per unit time, much lower than the time-averaged defense rate, which happens to be

$$\lim_{t \rightarrow \infty} \frac{1}{t} \mathbb{E}[N_d(t)] = \lambda - \lim_{t \rightarrow \infty} \frac{1}{t} \mathbb{E}[N_l(t)] = 93.21.$$

As the defense rate decreases, the expected surface size and exploitation rate increase sharply. At  $\alpha = 50\%$ , the expected surface size grows to 52.1% with a substantial breach rate of 69.69. This means, there are more than twice as many breaches as there are successful defenses. Breach rate grows even further to 84.16% as we further decrease the defense rate to 10%. The interesting thing here is that, the expected attack surface size in this final situation remains at 57.44, very close to the case with  $\alpha = 0.25$ , despite a significant decrease to  $\alpha = 0.1$ .

The above situation can be explained by the fact that, as the surface size grows, much of the departures are caused by a breach rather than a successful patch. As a result, the average surface size remains relatively static, however the instantaneous fluctuations above the mean are quickly exploited by the growing set of attackers. As a result, even though one may think that the attack surface is not much higher, the breach rate grows at a much higher pace with reduced defense rate.

Our initial results demonstrate a **phase-transition** phenomenon in the attack surface size distribution. Once the defense rate goes below a certain point, the surface distribution shifts sharply and abruptly to the right. Further reducing the defense rate beyond that shifting point does *not* change the distribution considerably. This observation underlines the importance of keeping a disciplined security posture for an organization and the resources should be allocated to have a rate at least identical to (if not much higher than) the rate of growth in vulnerabilities. For example, if the defense rate is set to  $\alpha = 200\%$ , the expected attack surface size remains below *a single vulnerability*, while the average breach rate is merely 0.29 per unit time! Our results show that a small increase in resources can substantially improve protection against breaches, whereas insufficient resource allocation leads to sharply degraded security performance.

## 5.2 AI-driven Dynamics

We continue the illustrative analysis with the memoryless model to study how AI-driven acceleration of vulnerability discovery and response affects attack-surface dynamics, captured through a simple rate-scaling abstraction. Let us introduce an *AI amplification factor* that scales the arrival and service rates and study its effect under symmetric and asymmetric amplification of attack and defense capabilities. We scale the vulnerability arrival rate and the exploitation rate by the same factor  $a$ , so  $\lambda \rightarrow a\lambda$  and  $\mu_l \rightarrow a\mu_l$ . In the second part, we will scale the defense rate  $\mu_d$  with the same rate, to evaluate the impact of the use of AI on the defensive side, as well as the attackers' side.

In this example, we use the same amplification factor across the three pillars of the model. Our intention here is to illustrate the drastic shift in temporal dynamics even when there is no change in the spatial dynamics of the surface. Also, we show the dynamics under asymmetry in AI amplification between attack and defense, where the asymmetry is in the favor of the attackers.

Similar to Section 5.1, we use  $\mu_d(t) = \alpha\lambda$ , where  $\alpha$  is the defense rate and  $\mu_l(t) = \beta\lambda N(t)$ . We provide the probability mass function for the attack surface for three different situations:

- (1) No AI is used (i.e.,  $a = 1$ ) on either the offense or the defense. Here, we choose the vulnerability arrival rate  $\lambda = 5$ , defense rate  $\alpha = 50\%$ , and the attack rate  $\beta = 0.005$ ;
- (2) AI used on the attack and defense with an AI amplification factor of  $a = 4$  on both sides. Here, the  $\lambda = 20$ , is amplified by  $a$  compared to the previous case and both the attack and defense resources are also benefiting the same rate of amplification.
- (3) AI is used on the attack side only. As a result, the overall defense resources remain at 2.5 units as in the original situation, while the vulnerability arrival rate and the attack rate scale with the AI amplification factor  $a = 4$ .

In Fig. 3, we illustrate the attack surface distributions for Cases (1-3) above. For Case 1 (no AI), the expected surface size remains at  $\mathbb{E}[N(t)] = 42.48\%$  at a defense rate of 2.5 patches per unit time while the exploit rate is 2.06 exploits per unit time.

Notably, when AI-driven acceleration is applied symmetrically to both attack and defense, the steady-state distribution of the attack surface remains unchanged, even though vulnerabilities arrive and are processed at a faster rate. However, all event rates scale with the amplification factor. In particular, *the exploitation rate increases from 2.06 to 8.24 exploits per unit time*, i.e., by a factor of  $a$ . Thus, while the shape of the attack-surface distribution is preserved, successful exploits occur more frequently due to the accelerated underlying dynamics. This observation highlights that symmetric acceleration primarily compresses the time scale of events rather than altering the distribution itself, and suggests that simply matching attack acceleration with defensive acceleration may be insufficient to reduce exploitation frequency.

442 Lastly, if the defense does not use AI, while the AI is used on the attack, the expected surface  
 443 size substantially increases to 80.54%. The exploitation rate is scaled up to 13.23 per unit time,  
 444 demonstrating a super-linear increase with AI amplification factor. This observation shows that  
 445 an asymmetry in the AI usage in the favor of the attack side leads to a disproportionately higher  
 446 increase in the rate of successful exploits. This scenario illustrates how asymmetric acceleration on  
 447 the attack side can significantly worsen backlog and exploit rates under fixed defense capacity.

448 The illustrative examples above demonstrate how fixed and AI-amplified defense rates influence  
 449 the steady-state behavior of the attack surface. We now turn to real-world data to assess whether  
 450 these modeled dynamics hold in practice. In the next section, we integrate empirical vulnerability  
 451 data from the open-source software repositories and validate our queueing-theoretic framework  
 452 against observed attack surface behavior.

## 453 6 Data Integration: Software Supply Chain

454 In this section, we evaluate the suitability of our queueing-based risk model using empirical  
 455 vulnerability data. Our goal is to assess how accurately the model captures the temporal dynamics  
 456 and structural properties of attack surface evolution in operational settings. If such validation fails,  
 457 the utility of the model in guiding practical defense strategies would be limited. Once the fit is  
 458 validated, the model can be used subsequently in defense and mitigation approaches.

459 To that end, we implement our framework in the use case of open-source software supply chain. In  
 460 our implementation, we use the ARVO dataset [19], which aggregates more than 4,000 reproducible  
 461 vulnerabilities from Google’s OSS-Fuzz infrastructure, spanning hundreds of large-scale open-  
 462 source C/C++ projects. Each record includes rich metadata such as report and fix timestamps,  
 463 sanitizer type (ASan, MSan, UBSan), crash category (for example, heap buffer overflow or use  
 464 after free), and severity level (low, medium, or high). This information enables precise event-level  
 465 tracking of vulnerability discovery and patching. The dataset’s granularity makes it particularly  
 466 well suited for queueing-based modeling: vulnerability disclosures correspond to *arrivals*, while  
 467 patch completions represent *service completions*.

468 Using this dataset, we first analyze the empirical dynamics of vulnerability arrival and departures,  
 469 demonstrating that our queueing-theoretic framework provides an accurate and interpretable  
 470 representation of real-world attack surface evolution. We then show that the queueing model  
 471 faithfully reproduces the observed queue size dynamics, confirming its validity as a realistic  
 472 abstraction of complex software ecosystems. We further characterize the heavy-tailed nature of both  
 473 arrival and service processes, which reveals a systemic bottleneck that slows patch deployment and  
 474 motivates the need for adaptive, data-driven defense strategies. In the next section, we build on these  
 475 findings and propose a RL-based dynamic defense allocation algorithm that optimally distributes  
 476 defensive effort to manage the attack surface size under resource and switching constraints.

### 477 6.1 Validating the Proposed Queueing Model on the ARVO Dataset

478 The following steps outline our complete empirical pipeline for constructing, segmenting, and  
 479 validating the queueing model on the ARVO dataset, thereby linking theoretical formulation with  
 480 real-world vulnerability dynamics.

481 **Step 1. Queue reconstruction and exploratory analysis:** We first align vulnerability dis-  
 482 covery and patching timestamps to reconstruct the time series of open vulnerabilities  $N(t)$ . The  
 483 ARVO dataset used here provides exceptionally high resolution, tracking over 4,410 vulnerabilities  
 484 across 260 unique open-source projects from December 2016 to May 2024. Each record includes  
 485 exact event-level timestamps for vulnerability discovery and patching, alongside critical metadata  
 486 such as severity (including 1,150 High-severity cases), detection sanitizer (e.g., asan, msan), and  
 487 specific crash types like Heap-buffer-overflow and Use-of-uninitialized-value. Figure 4 shows clear  
 488

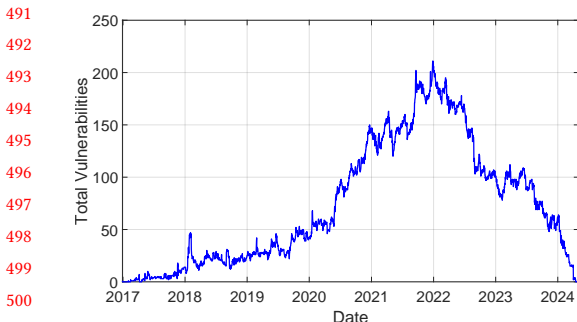


Fig. 4. Temporal evolution of the attack surface size,  $N(t)$ , in the ARVO dataset, showing bursty discovery, delayed patching, and non-stationary behavior.

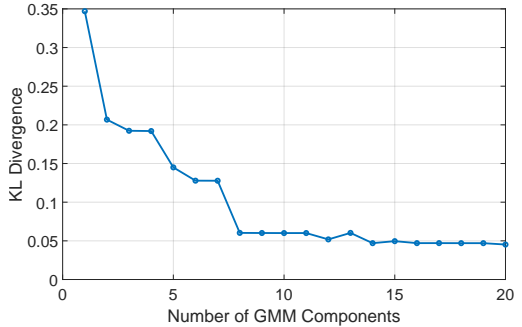


Fig. 5. KL divergence versus the number of Gaussian mixture components. Fit quality improves rapidly up to about ten components, after which additional components yield diminishing returns.

expansion and contraction phases, with bursty arrivals followed by delayed patching, confirming non-stationarity due to capacity limits in patching throughput.

**Step 2. Segmentation via Gaussian mixture modeling:** To capture these evolving patterns, we employed a *segmented modeling approach*. Segments are defined as mutually exclusive, closed intervals  $[t_{start}, t_{end}]$  that collectively partition the entire observation period. Within these intervals, the arrivals and departures are statistically analyzed in isolation from the rest of the dataset to uncover localized distribution shifts and non-stationarities in the time series. A Gaussian mixture model (GMM) fitted to the empirical QLD identified roughly ten quasi-stationary segments, each representing a distinct operational regime. The number of mixture components was selected based on the KL divergence elbow curve shown in Figure 5, which indicates that model fit improves sharply up to around ten components and then saturates. This segmentation enables locally stationary modeling of non-stationary dynamics.

**Step 3. Segment-wise parameter estimation:** Within each segment, we estimated inter-arrival and service distributions and calibrated the queue parameters  $(m, b)$  of a  $G/G/m-b$  model by minimizing the KL divergence between empirical and simulated QLDs. In this segmented setting, the parameter  $b$  represents the *mean available defensive resource* rather than the maximum capacity used in the next section, reflecting the average effective throughput observed in each operational regime. The resulting segmented models accurately reproduced the multimodal and time-varying dynamics of the attack surface, confirming that segmentation is essential for representing the non-stationary evolution observed in ARVO.

**Step 4. Statistical characterization of IA and ST:** After segmentation, we analyzed the stochastic structure within each stationary window to identify appropriate parametric distributions for inter-arrival ( $F_{IA}$ ) and service times ( $F_{ST}$ ). We evaluated a wide range of candidate distributions using five divergence metrics (KL, TVD, L2, JSD, and Wasserstein). Heavy-tailed mixtures consistently outperformed non-heavy-tailed models, such as the exponential distribution, which underestimated tail mass and failed to capture persistence effects. As illustrated in Figure 6, for the first segment (weeks 0–64), the best-fitting non-heavy-tailed model (exponential) yielded significantly higher KL divergences of 1.31 for IA and 1.34 for ST. In contrast, the heavy-tailed loglogistic and Gamma–InverseGaussian distributions achieved much lower KL divergences of approximately 0.77 and 0.42, respectively. These results confirm that both vulnerability discovery and patching processes are fundamentally heavy-tailed, justifying our use of more complex  $G/G/m$  abstractions to capture real-world long-lived exposure and temporal clustering.

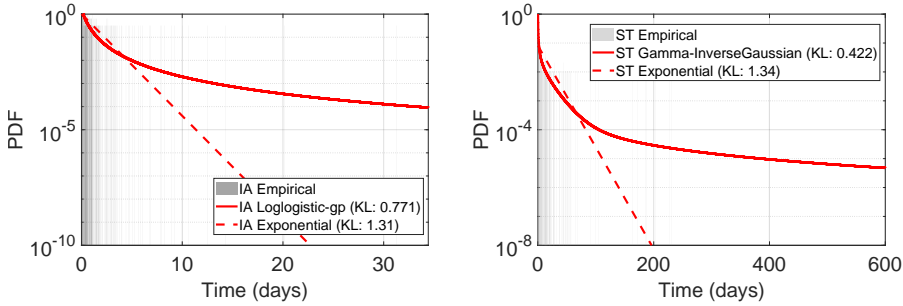


Fig. 6. IA and ST distributions for Component 1 (weeks 0–64). Loglogistic-general Pareto fits IA ( $KL \approx 0.77$ ); Gamma–InverseGaussian fits ST ( $KL \approx 0.42$ ).

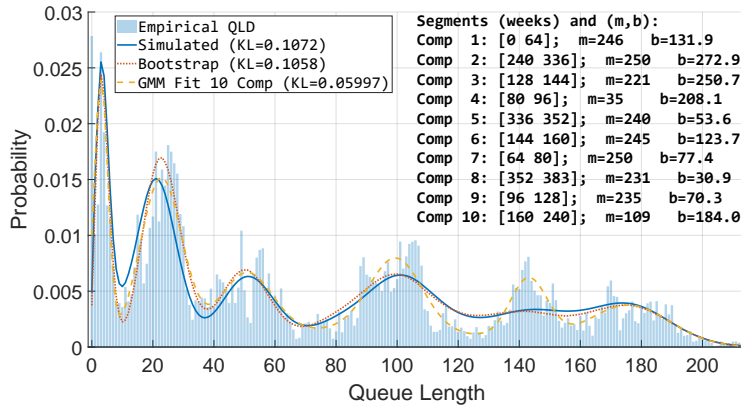


Fig. 7. Final integrated model: empirical QLD compared with segmented, bootstrap, and 10-component GMM fits. In the segmented  $G/G/m-b$  model,  $b$  denotes the mean available defensive resource rather than the maximum capacity used in the global formulation.

**Step 5. Segment-wise queue model fitting and validation:** Finally, we validate that the segmented  $G/G/m-b$  model accurately reproduces the empirical QLD observed in ARVO. Figure 7 compares the empirical QLD with the segmented, bootstrap, and ten-component GMM fits. In the bootstrap model, samples are drawn directly from the empirical data rather than from any fitted distribution, providing a nonparametric characterization. As shown, the segmented  $G/G/m-b$  model reproduces the empirical QLD with high fidelity, accurately capturing both the multimodal structure and the heavy-tailed persistence observed in practice. Quantitatively, the KL divergence between the empirical and simulated distributions is 0.1072, comparable to the nonparametric bootstrap (0.1058).

Across segments, the number of servers  $m$  remains relatively stable (220–250), while the effective resource capacity  $b$  varies widely (30–270), reflecting changes in patching throughput and organizational defense posture. Together, these results confirm that *empirically calibrated queueing abstractions replicate real-world attack surface dynamics with sub-0.11 KL divergence, demonstrating near-empirical precision*.

## 589    6.2 Temporal Characterization of Vulnerabilities of Software Releases

590    The empirical fits above confirm that vulnerability service times follow a heavy-tailed distribution,  
 591    with decay exponents ( $u$ ) in the range  $2 < u < 3$ . Consequently, vulnerabilities tend to remain  
 592    active on the attack surface for extended periods, depending on the underlying defense and exploit  
 593    dynamics. Our results are corroborated by prior measurements [15] on specific networks, in which  
 594    similar observations were made that the time a vulnerability remains exploitable follows a heavy-  
 595    tailed law with a tail in  $D_s$  that decays slowly in a non-exponential fashion. Building on this  
 596    empirical evidence, we formally show that when the vulnerability patching process exhibits such  
 597    heavy-tailed behavior, the attack surface size  $N(t)$  develops **long-range dependence (LRD)**, even  
 598    if the vulnerability arrival process itself is memoryless.

599    More specifically, let  $V(t)$  be memoryless with an arrival rate  $\lambda$  (a homogenous Poisson process  
 600    for simplicity in this section). Also, we define  $F(t)$  as the cumulative distribution function (cdf) of  
 601     $D_s$ , i.e., the service time<sup>2</sup>. A heavy-tailed distribution is characterized by a decay in  $1 - F(t)$ , that is  
 602    slower than  $t^{-u}$  for  $2 < u < 3$ .

603    **Theorem 1.** For memoryless  $V(t)$  and heavy-tailed  $F(t)$ , process  $N(t)$  is stationary and it exhibits  
 604    long-range dependence.

605    PROOF. See Appendix A for the complete proof. Here, we provide a sketch: our derivation begins  
 606    by establishing the autocovariance function of the number of customers in an M/G/ $\infty$  queue. We  
 607    prove that  $N(t)$  is wide-sense stationary and for heavy-tailed  $F(s)$ , the autocovariance function  
 608    decays slower than  $(\tau - t)^2$ , leading to a long-range dependent attack surface.  $\square$

609    LRD of the surface size implies that the impact of a vulnerability may last for an *extended*  
 610    amount of time. The size of the attack surface is not ergodic, making it extremely difficult for  
 611    the organization to control the cyber risk. That is, two different realizations of the process may  
 612    give completely different empirical statistics in terms of the attack surface dynamics. Therefore,  
 613    based on our analytical observation, an organization that regularly performs penetration testing to  
 614    identify, patch, and mitigate vulnerabilities can avoid long tails on the defense side, eliminating the  
 615    LRD and its negative side effects. Organizations should set up a security practice to ensure that the  
 616    vulnerability identification process occurs at regular (preferably deterministic) intervals.

617    Given that an organization has control over the distribution of inter-defense times, we next  
 618    develop a RL-based dynamic defense allocation algorithm to regulate the effective service times.

## 623    7 A Near-Optimal RL Algorithm for Adaptive Defense

624    Building on the model (Sec. 3) and the analytical insights into static allocation, temporal dependence,  
 625    and AI-driven dynamics (Secs. 5 and 6), we now build a systematic approach to the dynamic defense  
 626    problem. To that end, we present a near-optimal RL algorithm for adaptively allocating constrained  
 627    resources to dynamic defense, while accounting for switching costs. This learning-based approach  
 628    is needed because the arrival and service processes governing the attack surface are unknown and  
 629    may change over time. The RL agent represents an adaptive defender who episodically reallocates  
 630    limited patching or monitoring resources across a dynamic vulnerability queue. The transition  
 631    dynamics of the attack surface process are *unknown*. The policy switch for each episode corresponds  
 632    to an operational reconfiguration (e.g., retuning patching pipelines or reassigning response teams),  
 633    hence incurring measurable overhead modeled as a switching cost.

634  
 635  
 636    <sup>2</sup>For a vulnerability, we have that  $D_s = \min(D_d, D_e)$ .

## 638 7.1 Problem Setting and RL Framework

639 Specifically, this section provides the solution to the constrained optimization problem stated in (5),  
 640 where the defender seeks the optimal dynamic defense policy under uncertainty.

641 **Setting:** We apply the episodic Markov decision process (MDP) to model the dynamic defending  
 642 problem. As assumed in standard episodic MDPs, we consider  $H$  steps of interaction between the  
 643 defender and the attack surface in each episode<sup>3</sup>  $t = 1, \dots, T$ . At each step  $h = 1, \dots, H$ , based on the  
 644 observed state  $N^h(t)$  of the system, the defender can take a defense action  $\mu_d^h(t)$  according to a  
 645 policy  $\pi_t : \mathcal{N} \rightarrow \hat{\mu}_d$ , where  $\mathcal{N} = \{1, \dots, N\}$  is the system state space and  $\hat{\mu}_d = \{\mu_d\}$  is the defense  
 646 action space. The defense must satisfy the resource-budget constraint  $\mu_d^h(t) \leq b$  for all  $h$  and  $t$ .  
 647 After the defense action, the state evolves according to Eq. (1). The episodic formulation reflects  
 648 practical operation cycles, such as periodic defense planning or monitoring windows, during which  
 649 defense rates are adjusted based on observed backlog.

650 Given any state  $N^h$  at step  $h$ , the defense action given by the current policy  $\pi_t(\cdot)$  could be different  
 651 from that given by the policy  $\pi_{t-1}(\cdot)$  in last episode, in which case there will be a switching cost  
 652

$$653 \mathcal{S}^h(t, N^h) \triangleq w \cdot |\pi_t(N^h) - \pi_{t-1}(N^h)|$$

654 penalizing the change in defense across episodes, e.g., for parameter retuning, budget reallocation,  
 655 and recontracting. This cost captures the operational overhead of changing defense intensity,  
 656 rather than merely how often changes occur. Therefore, the goal is to find a desirable algorithm  $\pi$   
 657 that optimizes the expected cumulative penalty and defense cost over all steps and time-slots by  
 658 executing the policies  $\pi_{1:T}$ , i.e.,  $\min_{\pi_{1:T}} \sum_{t=1}^T [\mathcal{V}^{\pi_t} + \mathcal{S}^{\pi_t}]$ . Here, the  $\mathcal{V}$ -value function is defined to  
 659 be  
 660

$$661 \mathcal{V}^{\pi_t} \triangleq \mathbb{E} \left[ \sum_{h=1}^H \left[ C(N^h(t)) + \mu_d^h(t) \right] \right],$$

662 where the expectation is taken with respect to the randomness of the state transition (1) and the  
 663 race condition, and with a slight abuse of notation, the total switching cost is defined to be  
 664

$$665 \mathcal{S}^{\pi_t} \triangleq \mathbb{E} \left[ \sum_{h=1}^H \sum_{N^h \in \mathcal{N}} \mathcal{S}^h(t, N^h) \right]. \quad (6)$$

666 **Performance Metric:** We use the standard regret as the metric to evaluate the performance of RL  
 667 algorithm  $\pi$ , which is defined to be  
 668

$$669 \text{Reg}(T) \triangleq \sum_{t=1}^T [\mathcal{V}^{\pi_t} + \mathcal{S}^{\pi_t} - \mathcal{V}^*], \quad (7)$$

670 i.e., the difference between the expected cumulative cost of the RL algorithm  $\pi$  and the expected  
 671 cumulative cost  $\mathcal{V}^*$  of the optimal policy  $\pi^* = \arg \min_{\{\pi: \pi(N^h) \leq b, \forall h, N^h\}} \mathcal{V}^\pi$ . Note that the optimal  
 672 policy knows all problem parameters and does not change the policy. Thus, there is no switching cost  
 673 and we drop the round index  $t$ . Intuitively, this regret measures the cumulative excess vulnerability  
 674 exposure incurred by the learning defender relative to an omniscient optimal defense strategy.  
 675

676 **Novelties and Challenges:** To our knowledge, this work is the first to analyze RL with switching  
 677 costs that quantify the *magnitude* of policy change rather than merely the frequency of switching.  
 678 Specifically, the term  $\mathcal{S}^h(t, N^h)$  captures the absolute difference between consecutive defense  
 679 actions, measuring how much the policy changes over time. In contrast, existing RL formulations  
 680 penalize only whether  $\pi_t$  differs from  $\pi_{t-1}$ , without accounting for the extent of change [2, 10, 26].  
 681 Moreover, we address the new challenge arising from the simultaneous presence of switching costs  
 682 and resource-budget constraints, whose coexistence has not been studied in prior RL literature.  
 683

684 <sup>3</sup>Compared to the fixed allocation in traditional settings, this is a finer-grained setting where the defense action is taken in  
 685 a more dynamic way.

**Algorithm 1** Dynamic Defense Under Resource Constraints and Switching Costs

---

```

687
688 1: Parameters:  $\eta = \frac{1}{2H(H+1)}$  and  $c > 0$ 
689
690 2: Initialization:  $Q$ -value functions  $\tilde{Q}^h(N, \mu_d) = H$  and  $Q^h(N, \mu_d) = \tilde{Q}^h(N, \mu_d)$ , state-action
691     visitation counts  $N^h(N, \mu_d) = 0$ , where  $N$  represents the number of vulnerabilities in the
692     queue, and  $\mu_d$  represents the defense action
693 3: for  $t = 1 : T$  do
694    4:   for  $h = 1 : H$  do
695      5:        Take defense action
696         $\mu_d^h(t) = \arg \max_{\{\mu_d\}} Q^h(N^h(t), \mu_d)$ 
697      6:        Based on the arrivals of vulnerabilities and race condition, the queue state evolves to
698           $N^{h+1}(t)$  according to Eq. (1)
699      7:        Update the defense changing parameter
700         $k = N^h(N^h(t), \mu_d^h(t)) + 1$ 
701      8:        Update bonus  $\mathcal{B}(k) = c\sqrt{H^3/k}$  for defense exploration
702      9:        Update the estimate- $\tilde{Q}$ -value function according to Eq. (8).
703     10:       Update the estimate- $\tilde{V}$ -value function
704        $\tilde{V}^h(N^h(t)) = \min \left\{ H, \max_{\{\mu_d\}} \tilde{Q}^h(N^h(t), \mu_d) \right\}$ 
705     11:      if  $t \in \{t_n\}_{n \geq 1}$  then
706       12:         Update the belief- $Q$ -value
707          $Q^h(N^h(t), \cdot) = \tilde{Q}^h(N^h(t), \cdot)$ 
708     13:      end if
709   14:    end for
710 15:  end for

```

---

**7.2 Algorithm Design**

Our algorithm maintains two  $Q$ -value estimates. One is updated continuously to learn from new data, while the other is updated less frequently to determine defense actions and limit switching costs, which is detailed in Algorithm 1. The algorithm outlines the core RL update under delayed policy switching. The algorithm maintains an optimistic  $Q$ -estimate, updated periodically according to a geometrically increasing triggering sequence to balance responsiveness and stability. From a high-level point of view, we take the defense action according to an optimistic belief- $Q$ -value function. Specifically, at each step, our algorithm first updates an estimate- $\tilde{Q}$ -value function, which represents the value of taking a certain action at a state (line 9). An action with larger estimate- $\tilde{Q}$ -value function output is preferred. Intuitively, the belief- $Q$ -value function should be updated more frequently when the sample size is small (i.e., the uncertainty is large), and it should be updated less and less frequently when the sample size becomes larger and larger. To achieve this, a delayed belief- $Q$ -value function is updated when it has not been updated sufficiently long and triggers a switching threshold. Hence, to achieve effective defense with low switching costs, we need to carefully construct an effective belief- $Q$ -value function to guide the defense action and construct an elegant triggering time sequence  $\{t_n\}_{n \geq 1}$  for updating the belief- $Q$ -value function (lines 11-12), as well as for changing defense actions. Operationally, this design avoids frequent reconfiguration while still allowing rapid adaptation when uncertainty is high.

Specifically, in Line 7 of Algorithm 1, we first update the number of times the state  $N^h(t)$  and defense action  $\mu_d^h(t)$  are visited simultaneously, which will generate the bonus term in Line 8. This bonus term essentially captures the level of uncertainty after collecting  $k$  samples, such

that according to the concentration inequality (e.g., Hoeffding's inequality), the estimate- $\tilde{Q}$ -value function is an optimistic estimate of the optimal true  $Q$ -value with high probability. To guarantee this, we update the estimate- $\tilde{Q}$ -value function as follows,

$$\begin{aligned} \tilde{Q}^h(N^h(t), \mu_d^h(t)) &= (1 - \alpha(t))\tilde{Q}^h(N^h(t), \mu_d^h(t)) \\ &\quad + \alpha(t) \left[ (\bar{C} + b - C(N_l^h(t)) + \mu_d^h(t)) / (\bar{C} + b) \right. \\ &\quad \left. + \tilde{\mathcal{V}}^{h+1}(N^{h+1}(t)) + \mathcal{B}(k) \right], \end{aligned} \quad (8)$$

where  $\bar{C} = \sup\{C(\cdot)\}$ . This estimate- $\tilde{Q}$ -value is a weighted average between the old estimate- $\tilde{Q}$ -value  $\tilde{Q}^h(N^h(t), \mu_d^h(t))$  (for exploiting the knowledge learned from historical samples) and the newly learned knowledge from currently visited state-action pair

$$\begin{aligned} &\left[ (\bar{C} + b - (C(N_l^h(t)) + \mu_d^h(t))) / (\bar{C} + b) \right] \\ &\quad + \tilde{\mathcal{V}}^{h+1}(N^{h+1}(t)), \end{aligned} \quad (9)$$

together with a bonus term  $\mathcal{B}(k)$  (for encouraging exploration of potentially better defense strategies).

Finally, lines 11 and 12 determine whether or not to change the belief- $Q$ -value function that will directly determine the defense action  $\mu_d(t)$ . Let  $\tau(i) = \lceil (1 + \epsilon)^i \rceil$  for  $i = 1, 2, \dots$ , and define the triggering time sequence as

$$\{t_n\}_{n \geq 1} = [1, \tau(i_0)] \cup \{\tau(i_0 + 1), \tau(i_0 + 2), \dots\}, \quad (10)$$

where  $\epsilon$  and  $i_0 = \lceil \frac{\log(10H^2)}{\log(1+\eta)} \rceil$  are hyper-parameters chosen by the algorithm. For all  $t \in \{1, 2, \dots\}$ ,  $\tau_{\text{last}}(t) := \max\{t_n : t_n \leq t\}$  and  $\alpha(t) = \frac{H+1}{H+t}$ . The triggering time sequence (10) allows policy switch every time-slot at the beginning, and then the delay for policy switch keeps exponentially-increasing after a certain amount  $\tau(i_0)$  of samples has been collected. For example, the policy switches as follows. Given state  $N^h(t)$  at step  $h$ , we take some particular defense  $\mu_d^h(t)$  for time  $t$ , and update both the estimate- $\tilde{Q}$ -value and the belief- $Q$ -value immediately. After the time-slot  $\tau(i_0)$ , we still update  $\tilde{Q}$  immediately. However, we only update  $Q$  when  $t$  is in the triggering time sequence. This exponentially delayed update schedule enables high responsiveness early on and stability as uncertainty decreases, effectively balancing adaptation and switching cost.

### 7.3 Theoretical Regret Bound: Near-Optimality

We show that the proposed algorithm achieves near-optimal regret with high probability. In particular, with high probability  $1 - p$ , the theoretical regret of our algorithm is upper-bounded by  $\tilde{O}(\sqrt{T})$ , which is optimal. Recall that the regret is defined to compare our RL performance with the optimal policy, which is an oracle defender with full knowledge of system parameters and no switching penalty.

**Theorem 2. (Regret Upper-Bound)** With high probability  $1 - p$ ,  $p \in (0, 1)$ , the regret of Algorithm 1 is upper-bounded by  $\tilde{O}\left(\sqrt{H^3\bar{C}^4bT}\right)$  for any horizon  $T = \tilde{\Omega}(H^6\bar{C}^2b^2)$ .

**PROOF.** See Appendix B for the complete proof. Here, we provide a sketch. The proof follows optimism-based analysis for episodic RL, with new developments to handle the delayed defense switching and resource budgets. Let  $\tilde{Q}^h(t)$  denote the *estimate- $\tilde{Q}$ -value function*, which is continuously updated from new samples, and let  $Q^h(t)$  denote the *belief- $Q$ -value function*, a stabilized version used for policy decisions and updated only at triggering times  $\{t_n\}_{n \geq 1}$ . The proof involves the following key ideas.

(i) *Optimism and Concentration:* Each  $\tilde{Q}^h(t)$  update uses a step size  $\alpha(t) = \frac{H+1}{H+t}$  and an exploration bonus  $\mathcal{B}(k) = c\sqrt{H^3 \log(1/p')/k}$ . By standard concentration arguments (e.g., Azuma–Hoeffding inequality), with probability at least  $1 - p'$ , the estimate satisfies

$$0 \leq \tilde{Q}^h(t) - Q^{*,h} \leq \mathcal{B}(k) = \tilde{O}\left(\sqrt{\frac{H^3}{k}}\right),$$

uniformly over all  $(h, N, \mu, t)$ , where  $Q^{*,h}$  is the optimal  $Q$  value. This ensures *optimism*: the learned  $Q$ -values upper bound the true optimal values within  $\mathcal{B}(k)$ .

(ii) *Regret Decomposition:* Let  $\delta^h(t) = \tilde{V}^h(t) - V^{\pi_t,h}$  denote the instantaneous regret at step  $h$  in episode  $t$ . Since the policy  $\pi_t$  is derived from the most recently updated  $\tilde{Q}^h(k')$  at trigger  $k' \leq t$ , we decompose

$$\delta^h(t) \leq |(Q^h(k') - Q^{\pi_t,h})| + |\tilde{Q}^h(k') - Q^h(k')|,$$

where the first term behaves as in standard optimistic RL, while the second term measures the deviation caused by delayed updates.

(iii) *Controlling the Delay via Triggering Sequence:* Between two triggers,  $\tilde{Q}$  evolves according to small step sizes and bounded bonuses. Under the geometrically increasing triggering schedule  $t_n = \lceil(1+\epsilon)^n\rceil$ , the cumulative deviation  $\sum_t |\tilde{Q}^h(k') - Q^h(k')|$  grows at most by a constant factor  $1 + O(1/H)$  relative to non-delayed updates. Hence, the delay introduces only a multiplicative  $O(1/H)$  overhead.

(iv) *Error Propagation over the Horizon:* Summing the per-step inequalities and propagating value errors through the horizon yields

$$R^h \leq (1 + O(1/H))R^{h+1} + \tilde{O}(\sqrt{H^3 T}),$$

where  $R^h = \sum_t \delta^h(t)$ . Unrolling across  $h = 1, \dots, H$  gives  $\sum_h R^h = \tilde{O}(\sqrt{H^3 T})$ . Including bounded per-step costs  $\bar{C}$  and feasible budget  $b$  scales the bound to  $\tilde{O}(\sqrt{H^3 \bar{C}^4 b T})$ .

(v) *Switching Costs:* The number of belief- $Q$ -value updates, and hence policy changes, is logarithmic in time. Thus, the cumulative switching cost contributes at most  $\tilde{O}(\log T)$  to regret, absorbed by the main term.

Combining the above, the total regret then follows.  $\square$

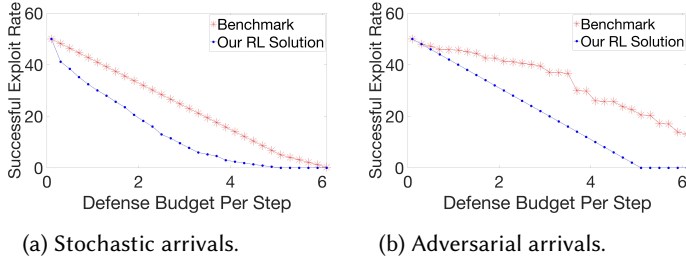
To the best of our knowledge, this is the first regret bound established for dynamic defense under the coexistence of resource-budget constraints and switching costs for amount of changes.

## 8 Numerical Evaluation

We now evaluate the proposed framework through a series of numerical experiments that combine model-based simulations and data-driven evaluations. These experiments evaluate how the RL defense policy performs under both synthetic and real-world conditions, focusing on attack surface size and exploitation rates. The analysis proceeds in three parts: (i) controlled model-based simulations to verify core dynamics, (ii) trace-driven evaluation using the ARVO dataset, and (iii) aggregate-budget simulations that examine RL reallocation under realistic resource constraints.

### 8.1 Model-based RL evaluation

We begin with controlled simulations based on the analytical model introduced in Section 4. These simulations evaluate the RL defense policy in a simplified environment where all system parameters are known. The results highlight two main effects: (i) the RL policy's ability to reduce successful exploits compared to fixed allocations, and (ii) its smoothing behavior under nonstationary vulnerability arrivals.



(a) Stochastic arrivals.

(b) Adversarial arrivals.

Fig. 8. Successful exploit rate vs. per-step defense budget (patches per unit time) under Model-based RL simulations.

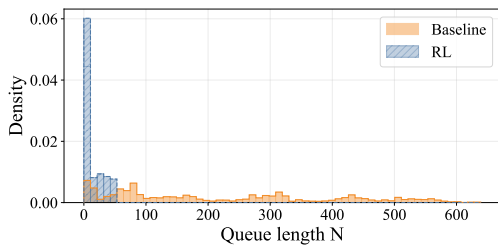


Fig. 9. Trace-driven comparison of queue-length probability densities on ARVO (RL vs. baseline) for per-step budget  $b = 1.0$  patches per unit time.

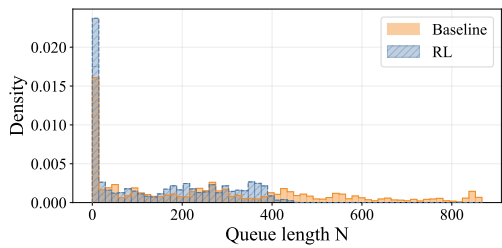


Fig. 10. Queue-length histogram under the empirical aggregate baseline budget and the RL-reallocated policy. Statistics are reported in the text.

**Setup:** We consider  $T = 10^4$  rounds, each with  $H = 10$  steps, and use the model  $\mu_\ell(t) = 3N(t)$  for exploitation rate in these runs. Vulnerability arrivals are drawn under two regimes: (i) *stochastic* arrivals with rate  $\lambda = 5$  at every step, and (ii) *adversarial* arrivals that vary arbitrarily in  $[0, 10]$ . We compare a fixed defending policy (constant per-step  $\mu_d$ ) to the learned policy produced by our RL procedure, sweeping the per-step defense budget  $b$  (measured in patches per unit time) and plotting the resulting successful exploit rates.

**Results:** Figure 8 shows successful exploit rate versus defense budget for the two arrival regimes. The learned policy reduces successful exploits substantially across budgets and attains up to a 55% reduction for certain budget points in the stochastic regime. In the adversarial regime, the learned policy both reduces the mean exploit rate and smooths high-frequency fluctuations compared to the fixed allocation, reducing both the mean exploit rate and its variability compared to the fixed allocation. The reduction in variability improving predictability of performance, thereby enables an organization to better plan their budget to achieve a specific goal against the attacks.

## 8.2 Trace-driven RL evaluation

We now evaluate the RL defense policy using a trace-driven simulator built from the ARVO dataset. Vulnerabilities arrive at each time step according to the ARVO records. The empirical per-step defended counts from ARVO define the trace-driven baseline. At each time step, the RL agent observes the current queue length (the number of active vulnerabilities) as the state and selects a defense-rate action. The simulator maps this rate to an integer number of defended vulnerabilities and updates the next state accordingly. We then compare the RL policy against the ARVO baseline.

**Setup:** We preprocess the ARVO data by binning records into 6-minute intervals; each bin is one time step and ten consecutive bins form an episode (one hour). This produces  $T = 64,395$  episodes.

883 Table 1. Trace-driven comparison statistics: queue-length mean &amp; variance (ARVO, RL vs. baseline).

885 Policy / Budget (patches per unit time)	Mean	Variance
886 Baseline (data)	219.9	30,930
887 RL (b=0.5)	59.4	1,602
888 RL (b=1.0)	13.0	219
889 RL (b=1.5)	4.7	56
890 RL (b=2.0)	1.2	6
891 RL (b=2.5)	0.1	0.4
892 RL (b=3.0)	0.1	0.3

894 Here, the defense budget  $b$  represents the maximum number of patches that can be applied per unit  
 895 time. We do not split the data into separate training and test sets; the full trace is used for learning  
 896 and we observe the result of the learning. For each bin, the number of reported vulnerabilities  
 897 is used as the stepwise arrival count, and the empirical defended counts in ARVO serve as the  
 898 baseline defense events. The RL agent observes only the arrivals and selects a defense-rate action;  
 899 the simulator maps that rate to an integer defended count via a Poisson draw and updates the next  
 900 state accordingly. The selected rate is converted to an integer defended count by drawing from  
 901 a Poisson distribution and truncating to the nearest nonnegative integer. At each step, both the  
 902 baseline and the RL defended counts (together with the arrivals) are applied to update the queue  
 903 state according to Eq. (1). The ARVO trace does not include separate attacker exploit events, so our  
 904 trace-driven evaluation considers only vulnerability arrivals and defenses.

905 The RL action space is  $\{0, 0.5, 1.0, 1.5, 2.0, 2.5, 3.0\}$  and at each step the agent selects a defense-rate  
 906 action  $\mu$  from this set. Because the agent is table-based, we set the maximum indexed queue size  
 907 for the Q-table to  $N_{\max} = 300$ ; if a larger queue is observed the agent still uses the  $N_{\max}$  index for  
 908 action selection, while we record the actual queue length for statistics. We use a per-step budget  $b$   
 909 (not an episode-level budget) and sweep  $b \in \{0.5, 1.0, 1.5, 2.0, 2.5, 3.0\}$  patches per unit time across  
 910 simulations. As each time step represents a 6-minute interval, a budget of  $b = 1.0$  corresponds  
 911 to an average capacity of 10 patches per hour. The optimistic bonus in the Q-value update is  
 912  $\mathcal{B}(k) = c_{\text{bonus}} \sqrt{H^3/k}$  with  $c_{\text{bonus}} = 0.1$ . To ensure a fair comparison, we tune a weight on the RL  
 913 defense cost so that the RL policy's total defended count over the full trace matches the empirical  
 914 baseline's total defended count. All other algorithmic settings follow Section 7.2.

915 **Results:** Figure 9 shows the queue-length density when per-step budget is  $b = 1.0$  patches per  
 916 unit time. For each budget  $b$ , we average results over 5 random seeds and report the queue-length  
 917 mean and variance for the RL policy and the baseline in Table 1. The RL policy consistently reduces  
 918 the queue length compared to the baseline, and the gains become larger as the per-step budget  
 919 increases.

### 920 8.3 Aggregate-budget RL reallocation

921 We next compare the baseline and RL when both use the same aggregate defense budget estimated  
 922 from the data in Figure 7. Specifically, we ask how queue-length performance changes if the RL  
 923 policy is allowed to reallocate, over time, the total defense rates used by the baseline.

924 **Setup:** Following Figure 7, we segment the ARVO trace into ten regimes and estimate the baseline  
 925 per-segment defense rates. In this subsection, we keep the ARVO arrivals unchanged and generate  
 926 the baseline defended counts by drawing Poisson samples with the estimated per-segment rates.  
 927 We then sum the baseline's defense rates over the full period to obtain its aggregate defense budget.  
 928 The RL operates as in Section 8.2 but is constrained so that its total defense effort over the full  
 929 930

period does not exceed this aggregate budget. This allows us to evaluate RL reallocation across steps under an equal total defense resource.

**Results (representative run):** Figure 10 plots the queue-length densities for the baseline (with the estimated defense rates) and for RL (with aggregate-budget reallocation). RL substantially reduces large queue lengths compared to the baseline. The summary statistics are  $\text{mean}(N) = 146.63$ ,  $N_{95} = 379$ , and  $N_{99} = 412.2$  for RL.  $\text{mean}(N) = 267.52$ ,  $N_{95} = 772$ , and  $N_{99} = 852$  for baseline. Thus, RL reallocation substantially reduces the mean queue length and shrinks the high-percentile tails of the distribution.

## 9 Discussion and Future Directions

We introduced a spatio-temporal queueing abstraction for the attack surface that models incoming vulnerabilities as arrivals and departures as either successful exploits or successful patches, and used this framework to derive several analytic insights. In particular, we highlight (i) a highly non-linear relationship between defense-resource shortfall and the rate of successful exploits, (ii) the emergence of long-range temporal dependence in the attack surface process when vulnerability lifetimes are heavy-tailed, and (iii) the fact that an aggregate AI-amplification of arrival and exploit rates can increase breach rates even when the attack surface distribution remains qualitatively similar.

While our analysis primarily focuses on a single-component system for clarity, the framework naturally extends to multi-component and multi-organizational settings. An organization's total attack surface can be viewed as a collection of correlated queues, each representing a subsystem such as authentication, storage, or cloud services. At a larger scale, an ecosystem of organizations can be modeled as a network of statistically dependent queueing systems, capturing interdependencies arising from shared software libraries, third-party integrations, or supply-chain relationships. For tractability, we restrict our formal analysis to the single-queue case, which already exhibits the essential dynamics of heavy-tailed persistence, feedback coupling, and resource constraints that characterize real-world attack surface evolution.

Building on these foundations, natural directions for future work include extending the queueing abstraction to **multiple, dependent queues** that reflect component structure; modeling the ecosystem of multiple organizations (and their interactions) as an interconnected queueing system; exploring collaborative defense formulations (e.g., multi-agent approaches) under resource constraints; and expanding empirical data collection to strengthen and validate the modeling assumptions.

## 10 Conclusion

We introduced a novel queueing-theoretic formulation to model the evolving cyber-attack surface, capturing both its temporal dynamics and spatial structure. Rather than following a narrow perspective that would focus on isolated attack vectors or specific vulnerabilities, our approach provides a holistic framework that reveals how systemic behaviors—such as heavy-tailed patching times—lead to long-range temporal dependencies in vulnerability exposure. The model also accommodates AI-induced amplification effects, allowing us to quantify the spatio-temporal dynamics of the attack surfaces under AI-generated threats and defenses. This dynamic queueing abstraction also lays the foundation for a principled defense allocation strategy, which we cast as a constrained sequential control problem and solve using reinforcement learning. We validated the framework using large-scale open-source vulnerability traces and show that an RL-based adaptive defense policy with near-optimal regret can reduce the mean attack surface size and the high-percentile tails under the same aggregate budget.

## 981 References

- [1] Sanae Amani, Christos Thrampoulidis, and Lin Yang. 2021. Safe reinforcement learning with linear function approximation. In *International Conference on Machine Learning*. PMLR, 243–253.
- [2] Yu Bai, Tengyang Xie, Nan Jiang, and Yu-Xiang Wang. 2019. Provably efficient q-learning with low switching cost. *Advances in Neural Information Processing Systems* 32 (2019).
- [3] Berkay Berabi, Alexey Gronskiy, Veselin Raychev, Gishor Sivanrupan, Victor Chibotaru, and Martin Vechev. 2024. DeepCode AI Fix: Fixing Security Vulnerabilities with Large Language Models. arXiv:2402.13291 [cs.CR]
- [4] Richard Fang, Rohan Bindu, Akul Gupta, Qiusi Zhan, and Daniel Kang. 2024. LLM Agents can Autonomously Hack Websites. arXiv:2402.06664 [cs.CR]
- [5] Andrew Feutrill, Matthew Roughan, Joshua Ross, and Yuval Yarom. 2020. A queueing solution to reduce delay in processing of disclosed vulnerabilities. In *2020 Second IEEE International Conference on Trust, Privacy and Security in Intelligent Systems and Applications (TPS-ISA)*. IEEE, 1–11.
- [6] Natarajan Gautam. 2012. Analysis of queues. *CRC Press, LLC, Boca Raton, Florida, United States* 10 (2012), 2222496.
- [7] Jonas Geiping, Alex Stein, Manli Shu, Khalid Saifullah, Yuxin Wen, and Tom Goldstein. 2024. Coercing LLMs to do and reveal (almost) anything. arXiv:2402.14020 [cs.LG]
- [8] Kaushik Haldar and Bimal Kumar Mishra. 2017. Mathematical model on vulnerability characterization and its impact on network epidemics. *International Journal of System Assurance Engineering and Management* 8, 2 (2017), 378–392.
- [9] Charles Harry, Ido Sivan-Sevilla, and Mark McDermott. 2025. Measuring the size and severity of the integrated cyber attack surface across US county governments. *Journal of Cybersecurity* 11, 1 (2025), tya032.
- [10] Jiawei Huang, Jinglin Chen, Li Zhao, Tao Qin, Nan Jiang, and Tie-Yan Liu. 2022. Towards deployment-efficient reinforcement learning: Lower bound and optimality. *arXiv preprint arXiv:2202.06450* (2022).
- [11] Xin Jin, Charalampos Katsis, Fan Sang, Jiahao Sun, Elisa Bertino, Ramana Rao Komppella, and Ashish Kundu. 2023. Prometheus: Infrastructure Security Posture Analysis with AI-generated Attack Graphs. arXiv:2312.13119 [cs.CR]
- [12] Jack A. Jones. 2011. FAIR - Factor Analysis of Information Risk. *Risk Management Insight LLC* (2011). <https://www.risklens.com/resources/fair-risk-analysis-model>
- [13] M. Khosravi-Farmad and A. Ghaemi-Bafghi. 2020. Bayesian Decision Network-Based Security Risk Management Framework. *Journal of Network and Systems Management* 28 (2020), 1794–1819. doi:10.1007/s10922-020-09558-5
- [14] Igor Kotenko, Diana Gaifulina, and Igor Zelenichenok. 2022. Systematic Literature Review of Security Event Correlation Methods. *IEEE Access* 10 (2022), 43387–43420. doi:10.1109/ACCESS.2022.3168976
- [15] Richard Lippmann and Daniel J Fried. 2005. Evaluating Intrusion Detection Systems: The 1998 DARPA Off-Line Intrusion Detection Evaluation. In *Recent Advances in Intrusion Detection*. Springer Berlin Heidelberg, 162–184.
- [16] Mingyan Liu. 2021. *Embracing Risk: Cyber Insurance as an Incentive Mechanism for Cybersecurity*. Springer.
- [17] Qisi Liu, Liudong Xing, and Chencheng Zhou. 2019. Probabilistic modeling and analysis of sequential cyber-attacks. *Engineering Reports* 1, 4 (2019). doi:10.1002/eng.212065
- [18] Pratyusa K. Manadhata and Jeannette M. Wing. 2011. An Attack Surface Metric. *IEEE Transactions on Software Engineering* 37, 3 (2011), 371–386. doi:10.1109/TSE.2010.60
- [19] Xiang Mei, Pulkit Singh Singaria, Jordi Del Castillo, Haoran Xi, Tiffany Bao, Ruoyu Wang, Yan Shoshitaishvili, Adam Doupé, Hammond Pearce, Brendan Dolan-Gavitt, et al. 2024. Arvo: Atlas of reproducible vulnerabilities for open source software. *arXiv preprint arXiv:2408.02153* (2024).
- [20] Daniel Miessler. [n.d.] AI Agents. [Link for the LinkedIn Post](#). Accessed: 2024-11-07.
- [21] Sobhan Miryoosefi and Chi Jin. 2022. A simple reward-free approach to constrained reinforcement learning. In *International Conference on Machine Learning*. PMLR, 15666–15698.
- [22] Federal Bureau of Investigation. 2024. FBI Warns of Increasing Threat of Cyber Criminals Utilizing Artificial Intelligence. [FBI Posting Link](#).
- [23] Nayot Poolsappasit, Rinku Dewri, and Indrajit Ray. 2012. Dynamic Security Risk Management Using Bayesian Attack Graphs. *IEEE Transactions on Dependable and Secure Computing* 9, 1 (2012), 61–74. doi:10.1109/TDSC.2011.34
- [24] Julie J.C.H. Ryan and Scott D. Dexter. 2009. A Bayesian Network Model for Predicting Cyber Security Threats. *Journal of Information Assurance and Security* 4, 2 (2009), 105–114. [https://www.mirlabs.org/jias/Volume4\\_2\\_2009/Vol4\\_2.html](https://www.mirlabs.org/jias/Volume4_2_2009/Vol4_2.html)
- [25] Abdulhakim Sabur, Ankur Chowdhary, Dijiang Huang, and Adel Alshamrani. 2022. Toward scalable graph-based security analysis for cloud networks. *Computer Networks* 206 (2022), 108795. doi:10.1016/j.comnet.2022.108795
- [26] Ming Shi, Yingbin Liang, and Ness Shroff. 2023. Near-optimal Adversarial Reinforcement Learning with Switching Costs. In *Eleventh International Conference on Learning Representations*.
- [27] Ming Shi, Yingbin Liang, and Ness Shroff. 2023. A near-optimal algorithm for safe reinforcement learning under instantaneous hard constraints. In *International Conference on Machine Learning*. PMLR, 31243–31268.
- [28] Robin Staab, Mark Vero, Mislav Balunović, and Martin Vechev. 2024. Large Language Models are Advanced Anonymizers. arXiv:2402.13846 [cs.AI]

- [29] Christopher Theisen, Nuthan Munaiah, Mahran Al-Zyoud, Jeffrey C Carver, Andrew Meneely, and Laurie Williams. 2018. Attack surface definitions: A systematic literature review. *Information and Software Technology* 104 (2018), 94–103.
- [30] H. Wang, D. Zhang, and S. Jajodia. 2008. An Attack-Graph Based Probabilistic Security Metric. In *IFIP Data and Applications Security '08*. Springer, 109–124. [https://link.springer.com/chapter/10.1007/978-0-387-09699-5\\_8](https://link.springer.com/chapter/10.1007/978-0-387-09699-5_8)
- [31] Yueqi Xie, Minghong Fang, Renjie Pi, and Neil Gong. 2024. GradSafe: Detecting Unsafe Prompts for LLMs via Safety-Critical Gradient Analysis. arXiv:2402.13494 [cs.CL]
- [32] Qi Zhang, Chunjie Zhou, Yu-Chu Tian, Naixue Xiong, Yuanqing Qin, and Bowen Hu. 2018. A Fuzzy Probability Bayesian Network Approach for Dynamic Cybersecurity Risk Assessment in Industrial Control Systems. *IEEE Transactions on Industrial Informatics* 14, 6 (2018), 2497–2506. doi:10.1109/TII.2017.2768998

## A Proof of Theorem 1

Let us define the indicator variable:

$$I_i(t) \triangleq \begin{cases} 1, & \text{a vulnerability arrives in } ((i-1)\delta, i\delta) \\ & \text{and still in the system at time } t \\ 0, & \text{otherwise} \end{cases}.$$

for  $\delta$  being the amount of temporal increment. Therefore,

$$N(t) = \sum_{i=-\infty}^{t/\delta} I_i(t). \quad (11)$$

For any  $t, \tau$  such that  $t \leq \tau$ ,

$$\begin{aligned} \mathbb{E}[N(t)N(\tau)] &= \mathbb{E}\left[\sum_{i=-\infty}^{t/\delta} \sum_{j=-\infty}^{\tau/\delta} I_i(t)I_j(\tau)\right] \\ &= \sum_{\{i \leq t/\delta, j \leq \tau/\delta \mid i \neq j\}} \mathbb{E}[I_i(t)I_j(\tau)] + \sum_{i=-\infty}^{t/\delta} \mathbb{E}[I_i(t)I_i(\tau)] \\ &= \sum_{\{i \leq t/\delta, j \leq \tau/\delta \mid i \neq j\}} \mathbb{E}[I_i(t)] \mathbb{E}[I_j(\tau)] + \sum_{i=-\infty}^{t/\delta} \mathbb{E}[I_i(t)I_i(\tau)], \end{aligned} \quad (12)$$

where Eq. (12) follows since  $I_i(t)$  and  $I_j(\tau)$  are independent for  $i \neq j$ . We can also write

$$\begin{aligned} \mathbb{E}[N(t)]\mathbb{E}[N(\tau)] &= \mathbb{E}\left[\sum_{i=-\infty}^{t/\delta} I_i(t)\right]\mathbb{E}\left[\sum_{j=-\infty}^{\tau/\delta} I_j(\tau)\right] \\ &= \sum_{\{i \leq t/\delta, j \leq \tau/\delta \mid i \neq j\}} \mathbb{E}[I_i(t)] \mathbb{E}[I_j(\tau)] \\ &\quad + \sum_{i=-\infty}^{t/\delta} \mathbb{E}[I_i(t)] \mathbb{E}[I_i(\tau)]. \end{aligned} \quad (13)$$

Combining Eq. (12) and (13) we get,

$$\begin{aligned} \text{cov}(N(t), N(\tau)) &= \mathbb{E}[N(t)N(\tau)] - \mathbb{E}[N(t)]\mathbb{E}[N(\tau)] \\ &= \sum_{i=-\infty}^{t/\delta} \{\mathbb{E}[I_i(t)I_i(\tau)] - \mathbb{E}[I_i(t)]\mathbb{E}[I_i(\tau)]\} \end{aligned} \quad (14)$$

$$= \sum_{i=-\infty}^{t/\delta} \{\lambda\delta[1 - F(\tau - i\delta)] - o(\delta)\}, \quad (15)$$

where the first term in (15) is due to  $\mathbb{E}[I_i(t)I_i(\tau)]$  and the  $o(\delta)$  is due to  $\mathbb{E}[I_i(t)]\mathbb{E}[I_i(\tau)]$  and that the probability of two vulnerabilities in the same instant is  $o(\delta)$ . As  $\delta \rightarrow 0^+$ ,

$$\text{cov}(N(t), N(\tau)) = \int_{-\infty}^t \lambda [1 - F(\tau - s)] ds = \lambda \int_{|\tau-t|}^{\infty} [1 - F(s)] ds. \quad (16)$$

Since the above covariance is a function of the time difference  $t - \tau$  only,  $\{N(t)\}$  is a stationary process. Thus, for heavy-tailed  $F(s)$ , the autocovariance function decays slower than  $(\tau - t)^2$ , leading to a long-range dependent attack surface.

## B Proof of Theorem 2

PROOF. For readability, we remove some indices when the context is clear. Recall that  $\tilde{Q}^h(t)$  denotes the *estimate-Q-value function*, continuously updated from new samples at step  $h$  and time  $t$ , while  $Q^h(t)$  denotes the *belief-Q-value function*, a stabilized version used to determine the defense action and updated only at triggering times  $\{t_n\}_{n \geq 1}$ .

**Step 1: Instantaneous regret decomposition:** Let  $\tilde{\delta}^h(t)$  be the instantaneous regret at step  $h$  and time  $t$ . Following the standard optimistic decomposition,

$$\begin{aligned} \tilde{\delta}^h(t) &= \left( \max \{ \tilde{Q}^h(t_\uparrow), \tilde{Q}^h(t) \} - Q^{*,h} \right)(N^h(t), \mu_d^h(t)) \\ &\leq |\tilde{Q}^h(t_\uparrow) - Q^{*,h}| + |\tilde{Q}^h(t) - \tilde{Q}^h(t_\uparrow)|, \end{aligned} \quad (17)$$

where  $t_\uparrow = \tau_{\text{last}}(t) + 1$  denotes the most recent triggering time before  $t$ . The first term corresponds to the standard value-estimation error, and the second term represents the additional deviation introduced by the delayed belief update.

**Step 2: Recursive relation for  $\tilde{Q}^h(t)$ :** The update of the estimate- $\tilde{Q}$ -value at visit  $t$  can be expanded as

$$\begin{aligned} \tilde{Q}_t^h(N, \mu_d) - Q^{\pi,h}(N, \mu_d) &= \alpha(t_i) \left( H - Q^{\pi,h}(N, \mu_d) \right) + \sum_{i=1}^k \alpha(t_i) \left[ C^h(N, \mu_d) \right. \\ &\quad + \tilde{V}_{t_i}^{h+1}(N_d^{h+1}(t_i)) - V^{\pi,h+1}(N^{h+1}(t_i)) \\ &\quad \left. + (\widehat{P}_{t_i}^h - P^h)V^{\pi,h+1}(N, \mu_d) + \mathcal{B}(t_i) \right], \end{aligned} \quad (18)$$

where  $\alpha(t_i)$  is the step size,  $B(t_i)$  is the exploration bonus, and  $\widehat{P}_{t_i}^h$  is the empirical transition model. This expression separates the stochastic update noise, transition deviation, and optimism term.

**Step 3: Bounding the delayed perturbation:** For any  $t > t_\uparrow$ , the cumulative drift between two consecutive triggers satisfies

$$\begin{aligned} |\tilde{Q}^h(t) - \tilde{Q}^h(t_\uparrow)|(N^h(t), \mu_d^h(t)) &\leq \phi_k + \sum_{i=\tau_{\text{last}}(t)+1}^t \alpha(t) \tilde{\zeta}_{t_i}^{h+1} + \bar{\zeta}_t^h, \end{aligned} \quad (19)$$

where  $\phi_k = O(\sqrt{H^3/k})$  and  $\bar{\zeta}_t^h = O(\sqrt{H^3/t})$  hold uniformly with high probability. Both terms can be absorbed into a constant multiple of  $\phi_k$ , since  $\phi_{t_\uparrow} \leq (1 + O(1/H))\phi_k$  under the geometric triggering rule.

1128 **Step 4: Coefficient aggregation:** When summing Eq. (19) over all time steps, each successor-state  
 1129 error  $\tilde{\zeta}_{t_\uparrow}^{h+1}$  is weighted by the accumulated step-size coefficients. Using the triggering sequence  
 1130  $t_n = \lceil (1 + \varepsilon)^n \rceil$  with  $\varepsilon = \frac{1}{2H(H+1)}$  and initial index  $r_0 = \lceil \frac{\log(10H^2)}{\log(1+\varepsilon)} \rceil$ , we obtain  
 1131

$$\begin{aligned} & \sum_t \left( \mathbf{1}\{\text{no trigger at } t\} \alpha(\tau_{\text{last}}(t)) + \mathbf{1}\{\text{trigger at } t\} \alpha(t) \right) \\ & \leq 1 + \frac{3}{H}, \end{aligned} \quad (20)$$

1136 showing that the delay inflates the propagation factor by at most  $(1 + 3/H)$ .

1137 **Step 5: Regret recursion and final bound:** Let  $R^h = \sum_t \tilde{\delta}^h(t)$ . Combining the above results yields  
 1138

$$R^h \leq (1 + O(1/H))R^{h+1} + \tilde{O}(\sqrt{H^3 T}).$$

1140 Unrolling the recursion over  $h = 1, \dots, H$  gives  $\sum_{h=1}^H R^h = \tilde{O}(\sqrt{H^3 T})$ . Accounting for the bounded  
 1141 per-step cost  $\bar{C}$  and defense-cap budget  $b$  scales the bound to  $\tilde{O}(\sqrt{H^3 \bar{C}^4 b T})$ . The number of belief-  
 1142  $Q$ -value updates, and hence policy changes, is logarithmic in time. Thus, the cumulative switching  
 1143 cost contributes at most  $\tilde{O}(\log T)$  to regret, absorbed by the main term.

1144  $\square$

1145

1146

1147

1148

1149

1150

1151

1152

1153

1154

1155

1156

1157

1158

1159

1160

1161

1162

1163

1164

1165

1166

1167

1168

1169

1170

1171

1172

1173

1174

1175

1176